Amit Pathak
Department of Mechanical Engineering,
University of California,
Santa Barbara, CA 93106

Robert M. McMeeking
Department of Mechanical Engineering,
University of California,
Santa Barbara, CA 93106;
Department of Materials,
University of California,
Santa Barbara, CA 93106;
INM Leibniz Institute for New Materials,
66123, Saarbruecken, Germany

Anthony G. Evans
Department of Mechanical Engineering,
University of California,
Santa Barbara, CA 93106;
Department of Materials,
University of California,
Santa Barbara, CA 93106

Vikram S. Deshpande
Department of Mechanical Engineering,
University of California,
Santa Barbara, CA 93106;
Department of Engineering,
University of Cambridge,
Trumpington Street,
Cambridge CB2 1PZ, UK

An Analysis of the Cooperative Mechano-Sensitive Feedback Between Intracellular Signaling, Focal Adhesion Development, and Stress Fiber Contractility

Cells communicate with their external environment via focal adhesions and generate activation signals that in turn trigger the activity of the intracellular contractile machinery. These signals can be triggered by mechanical loading that gives rise to a cooperative feedback loop among signaling, focal adhesion formation, and cytoskeletal contractility, which in turn equilibrates with the applied mechanical loads. We devise a signaling model that couples stress fiber contractility and mechano-sensitive focal adhesion models to complete this above mentioned feedback loop. The signaling model is based on a biochemical pathway where IP_3 molecules are generated when focal adhesions grow. These IP_3 molecules diffuse through the cytosol leading to the opening of ion channels that disgorge Ca^{2+} from the endoplasmic reticulum leading to the activation of the actin/myosin contractile machinery. A simple numerical example is presented where a one-dimensional cell adhered to a rigid substrate is pulled at one end, and the evolution of the stress fiber activation signal, stress fiber concentrations, and focal adhesion distributions are investigated. We demonstrate that while it is sufficient to approximate the activation signal as spatially uniform due to the rapid diffusion of the IP_3 through the cytosol, the level of the activation signal is sensitive to the rate of application of the mechanical loads. This suggests that ad hoc signaling models may not be able to capture the mechanical response of cells to a wide range of mechanical loading events.
[DOI: 10.1115/1.4003705]

Keywords: mechano-sensitivity, cell signaling, focal adhesions, actin/myosin contractility

1 Introduction

It is well known that living cells can sense mechanical stimuli. Forces applied to a cell or physical cues from the extracellular environment can elicit a wide range of biochemical responses that affect the cell's phenotype in health and disease (see, for example, reviews by Refs. [1–4]). Various mechanisms have been proposed to explain this phenomenon under different circumstances. These include changes in membrane fluidity that acts to increase receptor mobility and lead to enhanced receptor clustering and signal initiation [5,6], stretch-activated ion channels [7], mechanical disruption of microtubules [8], and forced deformations within the nucleus [9]. The most prevalent mechanism of mechanotransduction involves conformational changes in intracellular proteins along the force transmission pathway, connecting the extracellular matrix (ECM) with the cytoskeleton through focal adhesions [6,10,11]. For example, certain proteins that reside in "closed" conformation can be mechanically triggered to reveal their cryptic binding clefts upon the application of forces.

Force transmission from the extracellular matrix to the cell interior occurs through a chain of proteins called focal adhesions. These focal adhesions comprised an integrin-extracellular matrix protein bond (primarily vitronectin and fibronectin), integrin-associated proteins on the intracellular side (paxillin, talin, vinculin, etc.), and proteins linking the focal adhesion complex to the cytoskeleton. Stresses transmitted through adhesion receptors and distributed throughout the cell are thought to cause conformational changes in individual force transmitting proteins, any of which would be a candidate for force transduction into a biochemical signal. The process by which changes in protein conformation give rise to protein clustering at a focal adhesion or initiation of intracellular signaling, however, remains a current research area [12]. This active research has to date isolated a range of signaling pathways.

There is growing direct experimental evidence that mechanical loading triggers signaling cascades. For example, mechanical perturbation of the myocyte with an atomic force microscope (AFM) [13] results in IP_3-induced calcium release from intracellular stores and the propagation of a Ca^{2+} wave, as indicated by high speed video microscopy using fluorescent indicators of intracellular Ca^{2+} (see Fig. 1). Similar measurements have also been reported for Src waves induced by mechanical forces [14]. Independent measurements have also indicated that similar mechanical perturbations induce the formation and growth of focal adhesion complexes [15] and actin/myosin stress fiber arrangements [16] focused at or near the location of the application of the mechanical forces. These three phenomena, viz., signaling, focal adhesion formation, and cytoskeletal contractility, are closely linked in a cooperative feedback loop via a four step chain, as illustrated in Fig. 2.

Step 1. A mechanical perturbation of the cell membrane results

Contributed by the Applied Mechanics Division of ASME for publication in the JOURNAL OF APPLIED MECHANICS. Manuscript received May 7, 2010; final manuscript received October 7, 2010; accepted manuscript posted February 23, 2011; published online April 12, 2011. Assoc. Editor: Tayfun E. Tezduyar.

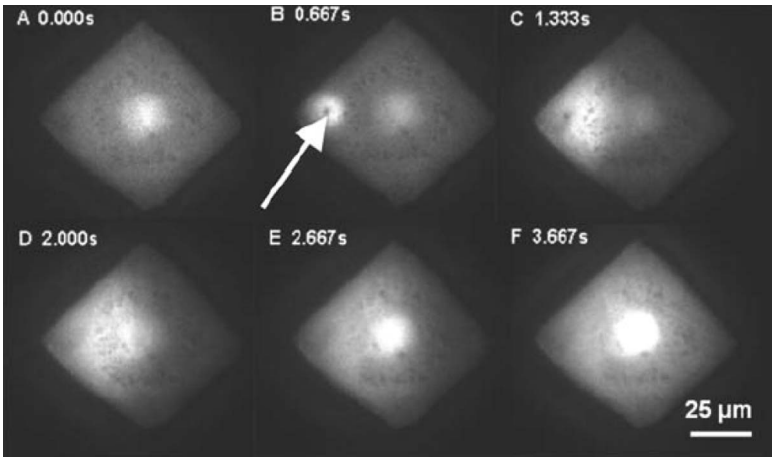

Fig. 1 A sequence of images showing the progression of a Ca^{2+} wave initiated by the mechanical perturbation of a cardiac myocyte by an AFM tip. The location of the AFM tip is indicated by the arrow. Adapted from Ref. [13].

in the formation and growth of focal adhesion complexes at highly stressed locations within the cell.

Step 2. The aggregation of proteins within the focal adhesion complexes triggers the signaling cascades of a range of signaling proteins and ions such as Rho, Src, and Ca^{2+}.

Step 3. These signaling molecules stimulate cytoskeletal contractility via the formation of actin/myosin stress fibers.

Step 4. The contractile forces generated by stress fibers apply forces on focal adhesions, which induces further aggregation of integrins in focal adhesions resulting in further signaling cascades and consequent cytoskeletal rearrangements.

The main focus of this paper is to lay out a framework that is capable of consistently modeling this cooperative loop among signaling, focal adhesion formation, and cytoskeletal contractility. In order to do so, we build on existing mechano-sensitive focal adhesion [17] and cell contractility models [18,19] to include the feedback loop involving intracellular signaling discussed above.

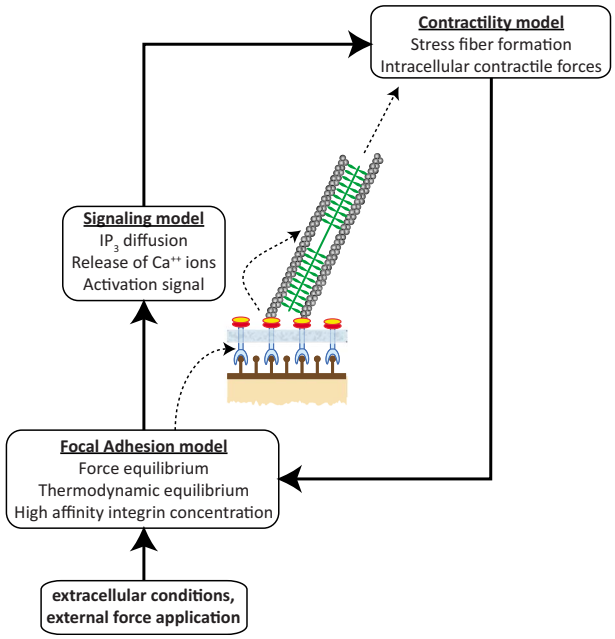

Fig. 2 Schematic illustrating the cooperative feedback loop between signaling, focal adhesion formation, and stress fiber contractility initiated by an external mechanical perturbation

The outcome will be a modeling approach capable of predicting the development of focal adhesion formation/dissociation, cytoskeletal remodeling involving actin/myosin stress fibers, and associated signaling cascades in response to the mechanical environment of a cell. Such a model would then be capable of modeling the response of cells to a range of mechanical perturbations, including stretching of cells via optical traps [20,21], poking by AFM tips, and micropipette aspiration [15,16].

2 Model for Signal Initiation and Transduction

A general review of the key biochemical processes governing focal adhesion formation, signaling (Fig. 3), and contractility is given in Appendix A. Based on the mechanisms described therein, the main aspects of the signal activation and transduction phenomena in the cell are (i) production of IP_3 due to the clustering of high affinity integrins, (ii) diffusion of IP_3 molecules through the cell, (iii) release of Ca^{2+} from endoplasmic reticulum (ER), and finally (iv) the activation of the intracellular contractile machinery, which in turn can instigate additional focal adhesion formation. In this section, we devise a signaling model that can be readily coupled with the stress fiber model of Refs. [18,19] and the associated focal adhesion model [17] in order to produce a comprehensive model for cellular contractility. Cartesian tensor notation is adopted throughout.

We emphasize here that details regarding the precise proteins involved in signaling are not crucial to the mathematical model detailed below. Rather, the structure of the reaction-diffusion scheme outlined below to propagate the signal from the focal adhesions to the intracellular contractile proteins is similar to that proposed for contractility mediated by Rho GTPase [22] and other signaling pathways involving ATP (adenosine-5'-triphosphate) and NO (nitric oxide)—the novelty of the treatment lies in the coupling of focal adhesion formation/dissociation with cellular contractility.

2.1 Model for IP_3 Production and Diffusion. The clustering of high affinity integrins initiates the production of IP_3, which diffuses through the cell. Simultaneously, IP_3 is being dephosphorylated by specific phosphatases to form IP_2 and IP_4. Denoting the concentration of IP_3 at a spatial coordinate x_i within the cytosol by S, these processes are described by the reaction-diffusion equation

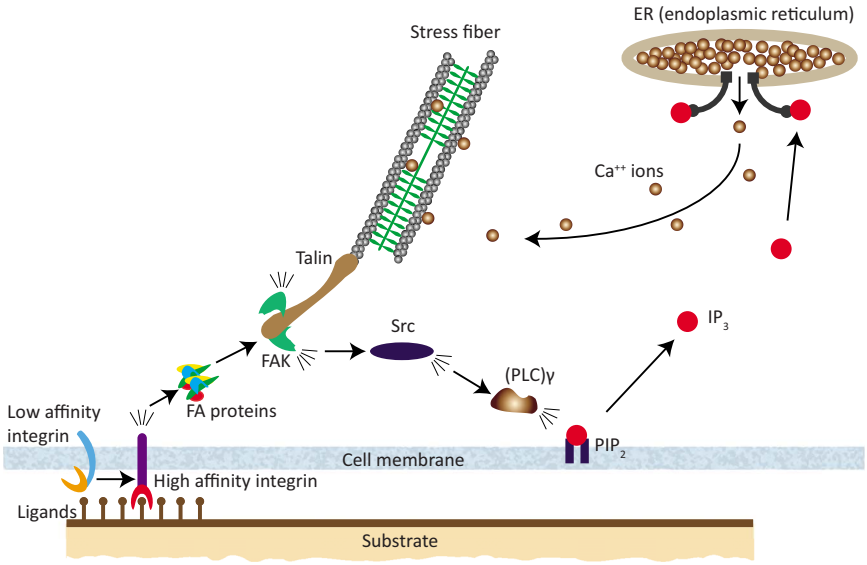

Fig. 3 A sketch illustrating the key biochemical processes involved in the signaling pathways induced by focal adhesion formation and resulting in the activation of the stress fiber contractile machinery

$$\dot{S} = m_s kT \frac{\partial^2 S}{\partial x_i^2} - k_d S - S\dot{\varepsilon}_{kk} \tag{2.1}$$

where the overdot denotes differentiation with respect to time. The flux boundary condition

$$m_s kT\left(n_i \frac{\partial S}{\partial x_i}\right) = -\alpha \max(0, \dot{\xi}_H) \tag{2.2}$$

over the cell membrane Γ with outward normal n_i along with the distribution $S(x_i)$ at time $t=0$ completes the specification of the reaction-diffusion equation. The variables and material properties in Eqs. (2.1) and (2.2) are described subsequently. The rationale of the three terms on the right hand side of Eq. (2.1) is as follows.

(i) The first term describes the diffusion of IP_3 through the cytosol, with S denoting the concentration of IP_3 in molecules per unit volume, m_s as the mobility of IP_3 molecules in the cytosol, k as Boltzmann's constant, and T as the absolute temperature.
(ii) We assume the de-phosphorylation of IP_3 into IP_2, and IP_4 is described by a first order reaction with a forward rate constant k_d and a negligible reverse reaction rate. This is modeled by the second term in Eq. (2.1).
(iii) The final term describes the change in the concentration of IP_3 due to the change in the volume of the cytosol, with $\dot{\varepsilon}_{kk}$ denoting the volumetric strain rate at the location x_i.

The boundary condition (2.2) prescribes the rate of production of IP_3 at locations on the cell membrane where high affinity integrins cluster. The rate of change of the concentration of high affinity integrins per unit cell membrane area is denoted by $\dot{\xi}_H$. An increase in ξ_H results in the production of IP_3 with a nondimensional proportionality constant α. Thus, α is interpreted as the number of IP_3 molecules produced when one low affinity integrin molecule is converted to its high affinity configuration. Note that the transformation of integrins from the high affinity to the low affinity state (resulting in a negative $\dot{\xi}_H$) does not contribute toward IP_3 production or de-phosphorylation, as guaranteed by Eq. (2.2). The rate $\dot{\xi}_H$ is an input to Eq. (2.2) and is specified by a separate focal adhesion model, e.g., Deshpande et al. [17].

2.2 Signal Generation From the Release of Ca^{2+} Ions. The concentration of IP_3 molecules in the cell at any location x_i and time t is calculated using Eqs. (2.1) and (2.2). Recall that IP_3 induces an opening of the gated channels of the Ca^{2+} stores in the ER, while Ca^{2+} is actively pumped back into the ER by molecular pumps on the walls of the ER. We express these kinetics in terms of the normalized Ca^{2+} concentration $C(0 \le C \le 1)$, where C is the ratio of the Ca^{2+} concentration to the maximum allowable concentration. Assuming first order kinetics, the rate of change of C at any location in the cytosol is given as

$$\frac{\partial C}{\partial t} = \lambda_f \frac{S}{S_0}(1 - C) - \lambda_b C \tag{2.3}$$

where λ_f is the rate constant governing the rate of release of Ca^{2+} from the IP_3-gated ER stores, and S_0 is a reference concentration of IP_3. Equation (2.3) guarantees that the release rate of Ca^{2+} ions is zero when $S=0$ (gated channels on the ER are closed) and increases with increasing S. The rate constant λ_b governs the rate at which Ca^{2+} is pumped back into the ER. The kinetic relation provides the value of the signal C at any location in the cytosol to initiate cytoskeletal stress fiber rearrangement; i.e., this is the input to a stress fiber model like that of Refs. [18,19]. The first order kinetics assumed in Eq. (2.3) means that the maximum (and steady-state) value of the cystolic Ca^{2+} is given by Eq. (3.10) (discussed subsequently). Thus, in general, the steady-state cystolic Ca^{2+} concentration is not equal to concentration of Ca^{2+} in the ER and set by the ratio of the rate constants λ_f and λ_b.

2.3 Coupling With the Stress Fiber and Focal Adhesion Models. The concentration of Ca^{2+} in the cytosol as parametrized by C results in the initiation of stress fiber formation. In this section, we specify how this is coupled with stress fiber and focal adhesion models using examples of the stress fiber models [18,19] and focal adhesion models [17]. In the stress fiber model of Refs. [18,19], they specify a kinetic equation for the formation and dissociation of stress fibers as

$$\dot{\eta} = [1 - \eta]Ck_f - \left(1 - \frac{\sigma}{\sigma_0}\right)\eta k_b \tag{2.4}$$

where $\eta(0 \le \eta \le 1)$ is defined as the ratio of the concentration of the polymerized actin and phosphorylated myosin within a stress

fiber bundle, at a particular orientation, to the maximum concentrations permitted by biochemistry. In Eq. (2.4), σ is the tension in the stress fiber bundle, while $\sigma_o \equiv \eta\sigma_{\max}$ is the corresponding isometric stress at the activation level η. The rate constants k_f and k_b are the stress fiber formation and dissociation rate constants. In the original model of Refs. [18,19], the signal C was specified in an ad hoc manner as an exponentially decaying signal of the form

$$C = \exp(-t/\theta) \tag{2.5}$$

where θ is the decay constant; i.e., the signal was not coupled to the formation of stress fibers or focal adhesions. As per the intracellular signaling analysis presented above, we replace Eq. (2.5) with C given by Eqs. (2.1)–(2.3). Thus, the signal resulting in the formation of stress fibers is directly coupled to the formation of focal adhesions.

The signal starts the formation of stress fibers and consequently results in stress generation within the cell. These stresses apply tractions T_i to the focal adhesions on the cell membrane to which they are attached. This lowers the chemical potential of the high affinity integrins, as discussed in Refs. [17,23]. The forces generated in the focal adhesions by their distortion, in turn, balance the stresses generated by the stress fibers, and thus the stress fiber organization controls the spatial and temporal development of the focal adhesions, as parametrized through the high affinity integrin concentration ξ_H over the cell membrane. The rate of increase in the focal adhesions, i.e., $\max(\dot{\xi}_H, 0)$, feeds back by generating the stress fiber activation signal C. Thus, it is the mechanical equilibrium of the cell that couples together signaling, stress fiber contractility, and focal adhesion formation. Specifically, the mechanical equilibrium of the cell is specified in terms of the stress Σ_{ij} as

$$\frac{\partial \Sigma_{ij}}{\partial x_j} = 0 \tag{2.6}$$

with traction boundary conditions $T_i \equiv \Sigma_{ij} n_j = \xi_H F_i$. Here, F_i is the force in a single high affinity integrin molecule, with the stress Σ_{ij} within the cytosol specified via the stress fiber contractility. On the other hand, the evolution of $T_i \equiv \xi_H F_i$ is given by the focal adhesion model.

We note that the generation of the contractility signal in this model is via the formation of focal adhesions, as described via Eqs. (2.1) and (2.2). Focal adhesions in turn can form due to mechanical perturbations (which lower the free energy of the high affinity integrins) or via a chemical stimulus such as the addition of serum into a cell culture. Thus, the model is capable of handling the contractile responses of cells to both mechanical or chemical stimuli.

3 Simulation of the Response of a Cell Under External Loading

In order to illustrate the capabilities of the model, here we present a simple numerical example of predictions of signaling cascades (and associated cell contractility) generated by mechanical perturbation in cells lying on stiff substrates. This choice of problem is motivated by numerous experimental data for such a scenario (see, for example, Ref. [13] (Fig. 1) and Ref. [14]). In future studies, the model will be exercised to predict the responses of cells for more complex (and physiologically relevant) boundary conditions such as the response of cells to substrate stretching and luminal fluid shear stress.

3.1 Formulation. Here, we illustrate the applicability of the model developed above in a simple one-dimensional setting. Consider a one-dimensional cell of thickness b, length L (along the x-direction), and unit thickness into the plane of the paper, bound to a long rigid substrate coated with an extracellular matrix (Fig. 4(a)). With x, the coordinate of a material point in the cell in the current configuration, and X, the corresponding coordinate in the undeformed configuration, a prescribed displacement rate $\dot{u}_{\text{app}}$ is applied to the right hand end ($X/L=1.0$). Using the model of Refs. [18,19] for describing the response of the cell interior (including the stress fibers) and the mechano-sensitive focal adhesion model of Ref. [17], the coupled signaling, adhesion, and contractile response of the one-dimensional cell is completely described by the following set of differential equations.

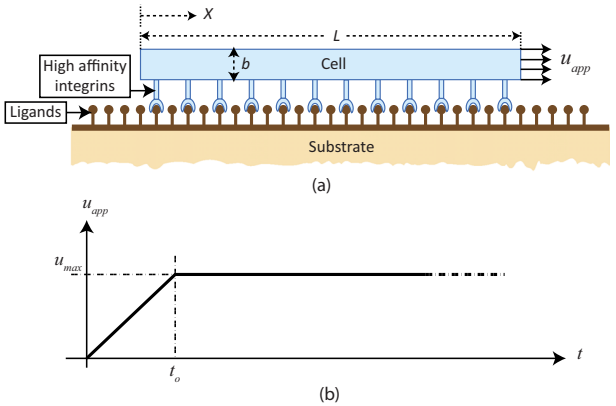

Fig. 4 (*a*) Sketch of the one-dimensional cell adhered to a rigid substrate. A prescribed displacement versus time history is imposed on one end of the cell. (*b*) The time history of the displacement u_{app} imposed on the cell in (*a*). The sketch defines the key loading parameters: the maximum applied $u_{\max}$ and the time t_o at which this displacement is reached.

(i) The one-dimensional mechanical equilibrium equation is

$$b\frac{\partial \Sigma}{\partial x} = \xi_H F \tag{3.1}$$

where F is the force exerted by the cell on the integrin-ligand complex and Σ is the stress in the cell, as specified in Appendix A via constitutive equations (B1)–(B3). These stresses follow from the stress fiber concentrations η. The boundary conditions for Eq. (3.1) are $\Sigma=0$ at $X=0$ with an applied displacement rate $\dot{u}=\dot{u}_{\text{app}}$ at $X=L$.

(ii) The strain-rate $\dot{\varepsilon}$ in the cell is related to the displacement rates $\dot{u}$ of cell material points through the compatibility equation

$$\dot{\varepsilon} \equiv \frac{\partial \dot{u}}{\partial x} \tag{3.2}$$

(iii) The integrin-ligand bond stretch rate $\dot{\Delta}$ is related to the cell displacement rate via

$$\dot{\Delta} = \begin{cases} \dot{u} & |\Delta| \le \Delta_n \text{ or } \left[\dfrac{\partial \Phi}{\partial |\Delta|}\dot{\Delta} < 0\right] \\ 0 & \text{otherwise} \end{cases} \tag{3.3}$$

where $\Phi(\Delta)$ is the stretch energy stored in the integrin-ligand complex and Δ_n is the stretch at maximum force. Assuming a quadratic form for Φ, the bond force F follows as

$$F \equiv \frac{\partial \Phi}{\partial \Delta} = \begin{cases} \kappa_s \Delta & |\Delta| \le \Delta_n \\ 2\kappa_s \Delta_n \operatorname{sgn}(\Delta) - \kappa_s \Delta & \Delta_n < |\Delta| \le 2\Delta_n \\ 0 & |\Delta| > 2\Delta_n \end{cases} \tag{3.4}$$

where κ_s is the stiffness of the integrin-ligand complex.

(iv) The one-dimensional trafficking equations for the concentration ξ_H of the high affinity integrins are

$$\frac{\partial \xi}{\partial t} = m\frac{\partial}{\partial x}\left(\xi_L \frac{\partial \chi_L}{\partial x}\right) - \xi\dot{\varepsilon} \tag{3.5}$$

where $\xi = \xi_L + \xi_H$ is the total integrin concentration given by the sum of the concentrations of the low affinity integrins (ξ_L) and the high affinity integrins (ξ_H). Here, m is the mobility of the low affinity integrins along the cell membrane, while χ_L is the chemical potential of a single low affinity integrin molecule. The thermodynamic equilibrium between the low and high affinity integrins dictates that [17]

$$\chi_L \equiv \mu_L + kT\ln\frac{\xi_L}{\xi_R} = \mu_H + kT\ln\frac{\xi_H}{\xi_R} + \Phi(\Delta) - F\Delta \tag{3.6}$$

where ξ_R is a reference binder concentration, while μ_L and μ_H are the reference potentials of the low and high affinity integrins, respectively. We solve these trafficking equations with the flux boundary condition $j = -m\xi_L(\partial\chi_L/\partial x) = 0$ at $X = 0, L$.

(v) The signal C is specified via one-dimensional versions of Eqs. (2.1)–(2.3); viz., the spatio-temporal evolution of the IP_3 concentration is given by

$$\dot{S} = m_s kT\frac{\partial^2 S}{\partial x^2} - k_d S + \frac{\alpha}{b}\max(0, \dot{\xi}_H) - S\dot{\varepsilon} \tag{3.7}$$

with the flux boundary condition $\partial S/\partial x = 0$ at $X = 0, L$, while the evolution of the stress fiber activation signal C is calculated from Eq. (2.3), with S obtained from the solution of Eq. (3.7).

For simplicity, we assume that the cell is stress and stress fiber free at time $t = 0$; thus, $u = \eta = \dot{\varepsilon} = C = S = \Sigma = 0$ throughout the cell at $t = 0$. Moreover, since the cells are initially stress free, the high affinity integrin-ligand complexes are unstretched such that $\Delta = 0$ everywhere on the cell surface. Then, Eq. (3.6) gives a uniform concentration of high and low affinity integrins over the cell surface at time $t = 0$, with ξ_L and ξ_H given by

$$\xi_H = \frac{\xi_o}{1 + \xi_L/\xi_H} \tag{3.8a}$$

and

$$\xi_L = \frac{\xi_o}{1 + \xi_H/\xi_L} \tag{3.8b}$$

respectively, where

$$\frac{\xi_H}{\xi_L} = \exp\left[-\frac{\mu_H - \mu_L}{kT}\right] \tag{3.9}$$

and ξ_o is the total integrin concentration per unit cell membrane area in an isolated cell.

An updated-Lagrangian finite element solution technique is used to solve these one-dimensional partial differential equations coupled together using a staggered approach similar to that described in Ref. [17]. All calculations use a mesh comprising 1000 two-node elements with linear interpolation functions. The mesh is refined near the edges, $X = 0, L$, in order to accurately capture large parameter gradients occurring there.

3.2 Material Parameters. We illustrate the features of the model by considering a one-dimensional cell, with thickness $b = 1$ μm and length $L = 10$ μm, adhered to a rigid substrate (Fig. 4(*a*)) at an ambient temperature $T = 310$ K. Unless otherwise stated, the relevant properties of the cell are as follows. The properties for the stress fibers and focal adhesion models have been chosen with guidance from previous assessments [17–19,23–25] and are consistent with a wide range of independent experimental measurements. The passive Young's modulus of the cell is $E = 0.08$ kPa and the Poisson's ratio is $\nu = 0.3$. The stress fiber formation/dissociation rate constants are $k_f = 1.4 \times 10^{-3}$ s^{-1} and $k_b = 0.1k_f$. The constants in the Hill-like equation relating the stress fiber stress to the strain rate are $\bar{k}_v = 6$, with $\dot{\varepsilon}_o = 2.8 \times 10^{-4}$ s^{-1}, while the maximum tension exerted by the stress fibers is $\sigma_{\max} = 3.9$ kPa. The concentration of integrins ξ_o over the cell membrane of an isolated cell is taken to be 3000 μm^{-2}, while the mobility of the low affinity binders is $m = 10$ s mg^{-1}. The difference in the chemical potential of the low and high affinity integrins is $\mu_H - \mu_L = 5kT$, and the stiffness of the integrin-ligand complex is chosen to be $\kappa_s = 0.015$ nN μm^{-1}. The maximum bond force that this complex can sustain is approximately 2 pN, and hence it follows that $\Delta_n = 130$ nm.

While the parameters for the stress fiber and focal adhesion models follow from previous studies, calibration assessments need to be conducted to establish appropriate ranges for the parameters of the signaling model. Here, we use the following values to demonstrate the capabilities of the model. Where possible, these parameters have been chosen to be consistent with experimental observations [26–28].

The reference IP_3 concentration is $S_o = 1000$ molecules μm^{-3} (i.e., ≈ 2 μM), while the forward and backward rate constants governing the release of Ca^{2+} are taken as $\lambda_f = 1$ s^{-1} and $\lambda_b = 0.5$ s^{-1}, consistent with values employed in Ref. [27]. We present parametric studies to show the effect of the following parameters: (i) the constant of proportionality α governing the rate of IP_3 production, (ii) the de-phosphorylation rate constant k_d, and (iii) the mobility m_s of the IP_3. Unless otherwise specified, we take the following parametric values as references: $k_d = 5 \times 10^{-4}$ s^{-1}, $\alpha = 1$, and the mobility of the IP_3, $m_s = 10^4$ s mg^{-1}.

We note that based on the parameter values stated above, the rate constants governing the release and capture of Ca^{2+} are significantly larger than the other rate relevant rate constants (e.g., the stress fiber formation/dissociation and IP_3 dephosphorylation). Given this, we expect the stress fiber activation signal to be temporally in phase with the IP_3 concentration and given by setting $\partial C/\partial t = 0$ in Eq. (2.3) to provide

$$C = \frac{1}{1 + \dfrac{\lambda_b}{\lambda_f}\dfrac{S_o}{S}} \tag{3.10}$$

3.3 A Simple Numerical Example. A displacement u_{app} is applied to the cell with a displacement versus time history, as sketched in Fig. 4(*b*). From time $t = 0$ to time $t_o = 1000$ s, a constant displacement rate $\dot{u}_{\text{app}} = 0.1$ nm s^{-1} in the positive X-direction (i.e., pulling of the cell) is applied, and subsequently ($t > 1000$ s), the cell edge $X = L$ is held fixed at the displacement $u_{\max} = 100$ nm with $\dot{u}_{\text{app}} = 0$. As no external biochemical signal is specified, the applied mechanical perturbation produces the activation signal that initiates the formation and growth of stress fibers and focal adhesions. The spatio-temporal evolution of the stress fiber activation signal C is shown in Fig. 5 for five selected values of time t (note that the distribution of C is plotted in terms of the undeformed cell coordinate X). The signal C tends to remain more localized near the displaced end of the cell, while $\dot{u}_{\text{app}} > 0$ (see the distribution of C at $t = 5$ min in Fig. 5) due to signal production near the location of applied load. Thereafter, the signal spreads uniformly throughout the cell shortly after time $t = t_o$ (see $t = 17$ min in Fig. 5) and subsequently gradually decays to zero in a spatially uniform manner. The signal is virtually nonexistent approximately 17 h after the initiation of the mechanical perturbation. As discussed in Sec. 3.2, the IP_3 is temporally in phase with the stress fiber activation signal, and thus the concentration $S(X,t)$ can be extracted from Fig. 5 using the relation Eq. (3.10).

The spatio-temporal distribution of the stress fiber concentration η and the focal adhesions as parametrized by ξ_H/ξ_o are plotted in Figs. 6(*a*) and 6(*b*), respectively. Early in the deformation

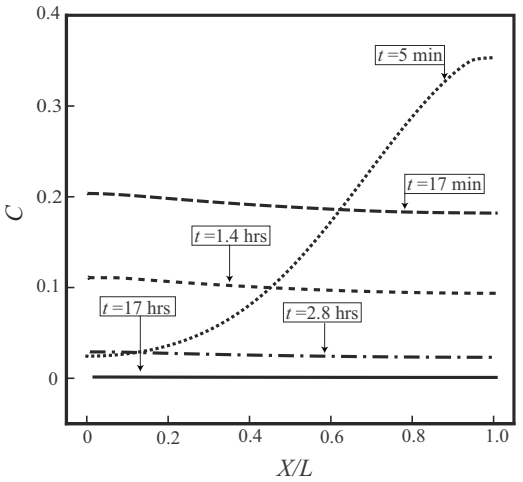

Fig. 5 The spatio-temporal evolution of the stress fiber activation signal *C* in the cell (reference properties) subjected u_{max} =100 nm at a displacement rate $\dot{u}_{app}$=0.1 nm s^{-1}. The spatial distributions are plotted in terms of the undeformed cell coordinate *X* at five selected times *t* after the initiation of the mechanical perturbation.

($t \leq 17$ min), both the stress fiber and focal adhesions are concentrated near the cell edge being pulled (i.e., $X=L$). Subsequently, η acquires approximately a uniform spatial distribution over the range $X/L>0.1$ and rises steadily with increasing time before reaching its final value of $\eta \approx 0.8$. Near the free edge $X=0$, η drops sharply as the $\Sigma=0$ boundary condition at that edge implies that the stress fiber concentration has to drop to zero as the strain rate $\dot{\epsilon} \to 0$ as the cell approaches a steady-state limit. By contrast, at times $t>17$ min, focal adhesions start to form near the free edge of the cell as mechanical equilibrium dictates that high tractions are developed by the stress fibers near the free edges of a cell, as discussed in Ref. [17]. Moreover, the diffuse focal adhesions near $X=L$ dissociate and concentrate in the immediate vicinity of the load application point $X=L$. This prediction is consistent with experimental observations [29], which show that focal adhesions, as measured by the vinculin concentration, form near the site of force application. Moreover, focal adhesions are seen to form over the region $X/L<0.1$, where the stress fiber concentration is rather low but has a strong gradient. This strong gradient in stress fiber concentration implies that the cell exerts large tractions on the substrate via focal adhesions. Given that the focal adhesions are mechano-sensitive, this results in the formation of focal adhesions in this region.

The spatial distributions of C, η, ξ_H/ξ_o, and the low affinity integrins ξ_L/ξ_o at $t=17$ h are plotted in Fig. 6(*c*). The spatial distribution of the mobile (low affinity) integrins is approximately uniform, indicating that the cell has nearly attained its steady-state configuration by this time whereupon there is no further focal adhesion and stress fiber formation. Removal of the applied displacement (and hence the applied end force) will result in the dissociation of the focal adhesions and stress fibers and the cell returning to its resting (initial) state. This result is not included here for the sake of brevity.

3.4 Significance of Diffusion of the Signal. Experimental measurements [26,28] suggest that the diffusivity of IP_3 is in the range $D_s \equiv m_s kT = 200-400$ μm^2 s^{-1} at $T=310$ K. Assuming a value of $D_s=400$ μm^2 s^{-1}, we anticipate that the IP_3 will diffuse over the cell of length $L=10$ μm for times $t>L^2/(4D_s) \approx 0.06$ s. All other time scales in the coupled stress fiber/focal adhesion equations are significantly longer (e.g., the time for the diffusion of the low affinity binders over the entire cell length is about 17 h, while the loading is applied over 1000 s). It thus

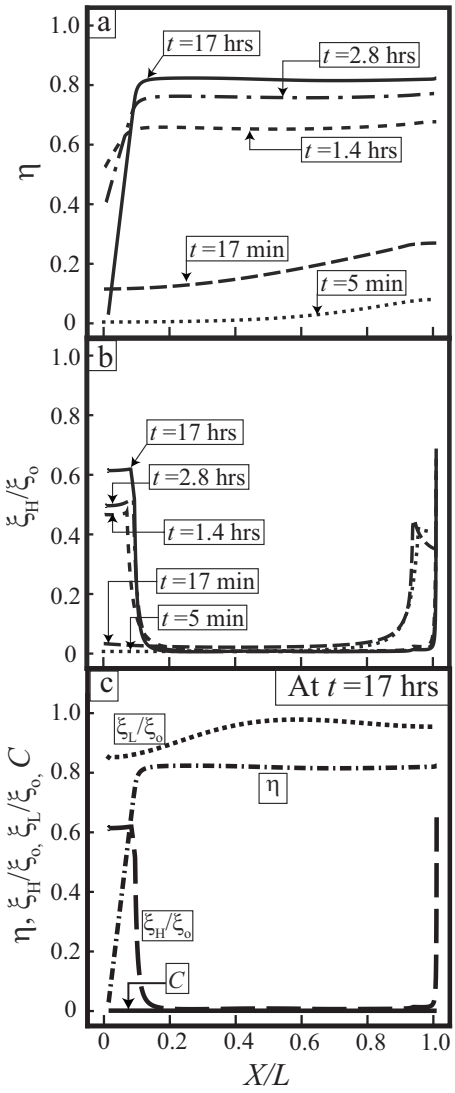

Fig. 6 The spatio-temporal distribution of the (*a*) stress fiber concentration η and (*b*) focal adhesions as parametrized by ξ_H/ξ_o in the cell (reference properties) subjected u_{max} =100 nm at a displacement rate $\dot{u}_{app}$=0.1 nm s^{-1}. The spatial distributions are plotted in terms of the undeformed cell coordinate *X* at five selected times *t* after the initiation of the mechanical perturbation. (*c*) The corresponding spatial distributions of *C*, η, ξ_H/ξ_o, and the low affinity integrins ξ_L/ξ_o at approximately steady-state (*t*=17 h).

seems appropriate to assume that over time scales of interest, the IP_3 concentration is spatially uniform. The model equations outlined in Sec. 4.1 are then modified as follows. The evolution equation for a spatially uniform IP_3 concentration $\bar{S}$ is given by an equation analogous to Eq. (3.7) as

$$\frac{\partial \bar{S}}{\partial t} = -k_d \bar{S} - \frac{\bar{S}}{L}\int_0^L \dot{\epsilon} dX + \frac{\alpha}{bL}\int_0^L \max(0, \dot{\xi}_H) dX \qquad (3.11)$$

This definition ensures global consistency between S and $\bar{S}$ such that

$$\frac{\partial \bar{S}}{\partial t} \equiv \frac{1}{L}\int_0^L \frac{\partial S}{\partial t} dX \qquad (3.12)$$

for a given distribution of $\dot{\xi}_H$ and $\dot{\epsilon}$ with zero flux boundary conditions at $X=0,L$. We replace S in Eq. (2.3) with $\bar{S}$ to give a

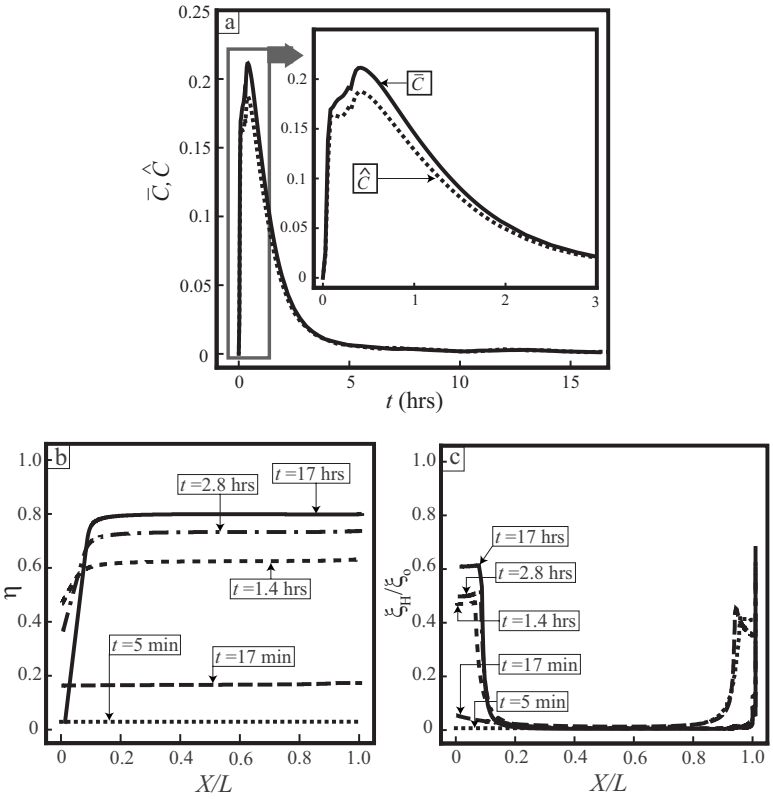

Fig. 7 (*a*) Comparison of temporal evolution of the signals $\hat{C}$ and $\bar{C}$ in a cell (reference properties) subjected u_{max}=100 nm at a displacement rate $\dot{u}_{app}$=0.1 nm s^{-1}. The corresponding spatio-temporal evolution of the (*a*) stress fiber concentration η and (*b*) focal adhesions as parametrized by ξ_H/ξ_o in the cell with infinitely rapid IP_3 diffusion (i.e., cell subjected to the signal $\hat{C}$). The spatial distributions are plotted in terms of the undeformed cell coordinate *X* at five selected times *t* after the initiation of the mechanical perturbation.

spatially uniform stress fiber activation signal denoted by $\hat{C}$.

The mechanical perturbation simulation described in Sec. 3.3 is repeated with this new formulation for a spatially uniform signal. The resulting temporal evolution of $\hat{C}$ (which by definition is spatially uniform) is plotted in Fig. 7(*a*). Recall that in the simulation presented in Sec. 3.3, we had taken D_s as 0.043 μm^2 s^{-1} (at a temperature T=310 K). It is instructive to compare the temporal evolution of the signal with this rather low diffusivity value with predictions where the diffusivity is taken to be infinitely large. In order to make this comparison, we define a spatial average of C as

$$\bar{C} \equiv \frac{1}{L}\int_0^L C dX \tag{3.13}$$

so that $\bar{C}=\hat{C}$ *if and only if S* is spatially uniform. The temporal evolution of $\bar{C}$ is included in Fig. 7(*a*) (with the inset showing the early time evolution of both $\hat{C}$): With $\bar{C}$ nearly equal to $\hat{C}$, our simulations suggest that the spatially uniform signal approximation is appropriate over all realistic values of the IP_3 diffusivity. Consistent with this finding, we observe that spatio-temporal evolutions of η and ξ_H/ξ_o in Figs. 7(*b*) and 7(*c*), respectively, using $\hat{C}$ as the stress fiber activation signal, are almost identical to the corresponding distributions plotted in Fig. 6, where diffusion of IP_3 was accounted for and C was used as the stress fiber activation signal.

We conclude that for purposes of modeling the stress fiber and focal adhesion evolution in response to a mechanical perturbation, it suffices to neglect the diffusion of IP_3 and employ a spatially uniform stress fiber activation signal. In all the simulations, presented subsequently, we employ the spatially uniform signal $\hat{C}$.

3.5 Sensitivity to the Parameters Governing the Production and De-Phosphorylation of IP_3. We now investigate the sensitivity of the stress fiber and focal adhesion response to the IP_3 production and de-phosphorylation parameters α and k_d, respectively. Unless otherwise specified, all cell and applied loading parameters are the same as in Sec. 3.4, i.e., the spatially uniform signal $\hat{C}$ with the mechanical perturbation applied, as specified in Sec. 3.3. The temporal variation of $\hat{C}$ for three choices of the IP_3 production proportionality constant α is shown in Fig. 8(*a*): With increasing α, both the peak value of $\hat{C}$ and the decay time of the signal increase. Consequently, both η and ξ_H/ξ_o increase with increasing α, as illustrated by the steady-state (t=17 h) distributions of these quantities plotted in Figs. 8(*b*) and 8(*c*), respectively.

The effect of k_d is very similar to α except that in this case the signal $\hat{C}$ (as well as η and ξ_H/ξ_o) increases with decreasing k_d as this reduces the rate of de-phosphorylation of IP_3. For the sake of brevity, these results are not shown explicitly.

4 Can We Decouple the Signaling Cascade From the Stress Fiber and Focal Adhesion Responses?

A key question is whether models such as those of Refs. [18,19], which prescribe a signal independent of the applied me-

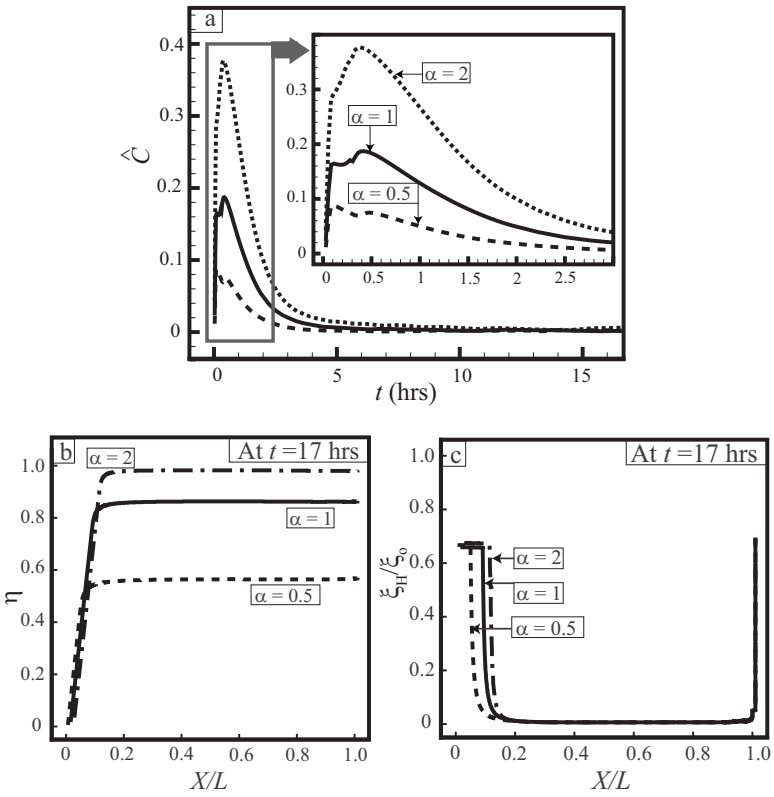

Fig. 8 (*a*) The temporal evolution of $\hat{C}$ in a cell subjected u_{max} =100 nm at a displacement rate $\dot{u}_{app}$=0.1 nm s^{-1} for three selected values of the IP$_3$ production constant α. All other values of the cell properties are fixed at their reference values. The corresponding steady-state (t=17 h) distributions of (*b*) stress fiber concentration η and (*c*) focal adhesions as parametrized by ξ_H/ξ_o. The spatial distributions are plotted in terms of the undeformed cell coordinate X.

chanical perturbations, are capable of capturing the resulting stress fiber and focal adhesion distributions. In order to address this question, we now report simulations where we investigate the influence of (i) the loading rate and (ii) the net applied displacement on the cellular response, including the generated stress fiber activation signal and the resulting stress fiber and focal adhesion distributions. All results are presented for a cell of length L =10 μm and an infinitely fast IP$_3$ diffusion rate, i.e., a spatially uniform activation signal $\hat{C}$. All other material parameters are kept fixed at their reference values, as specified in Sec. 3.2.

4.1 Effect of Loading Rate. A displacement schedule, as sketched in Fig. 4(*b*), was applied to the cell at $X=L$. Keeping the maximum displacement u_{max} fixed at 100 nm, the applied displacement rate during the initial loading period was varied from $\dot{u}_{app}$=0.02 nm s^{-1} to 0.5 nm s^{-1}; i.e., time t_o was reduced from 5000 s to 200 s. The resulting temporal variation of $\hat{C}$ is included in Fig. 9(*a*) for three selected values of $\dot{u}_{app}$. Clearly, the maximum value of $\hat{C}$ increases with increasing $\dot{u}_{app}$, while the time for $\hat{C}$ to attain this maximum value decreases. We note that the rise time for $\hat{C}$ scales with the time over which the applied displacement increases; i.e., the rise time scales with t_o and hence increases with decreasing $\dot{u}_{app}$. However, the decay time for the signal to fade away is mainly characterized by the dephosphorylation time constant k_d and hence is reasonably independent of the applied loading rate. A consequence of the higher signal levels with increasing $\dot{u}_{app}$ means that the steady-state (t =17 h) stress fiber concentrations are higher over the majority of the cell length for the higher values of applied $\dot{u}_{app}$ (Fig. 9(*b*)), but these increased signal levels have a negligible effect on the steady-state focal adhesion distributions (Fig. 9(*c*)), which saturate based on the maximum force that an integrin-ligand bond can sustain. We emphasize here that the results indicate that the concentration of stress fibers is not very sensitive to the loading rate. However, consistent with observations [30], the stress exerted by the fibers depends strongly on the rate of deformation, as characterized by Eq. (B2).

4.2 Effect of the Applied Net Displacement. Now, we keep the initial loading rate fixed at $\dot{u}_{app}$=0.1 nm s^{-1} and increase u_{max} from 100 nm to 500 nm by increasing t_o. The resulting temporal variation of the stress fiber activation signal $\hat{C}$ is plotted in Fig. 10 for three selected values of u_{max}. The activation signal and, consequently, the distributions of η and ξ_H/ξ_o (not shown) are seen to be insensitive to u_{max} over the range investigated here.

These findings seem to suggest that in order to make accurate predictions over a wide range of applied mechanical perturbations, the signaling model needs to be coupled to the stress fiber and focal adhesion model. Further, two- and three-dimensional investigations with more realistic cell geometries are required to judge under what circumstances it might be appropriate to decouple the signaling response of the cell as in Refs. [18,19].

5 Concluding Remarks

We have developed a model for mechano-sensitive signaling pathways in cells that give rise to a cooperative feedback loop between signaling, focal adhesion formation, and cytoskeletal

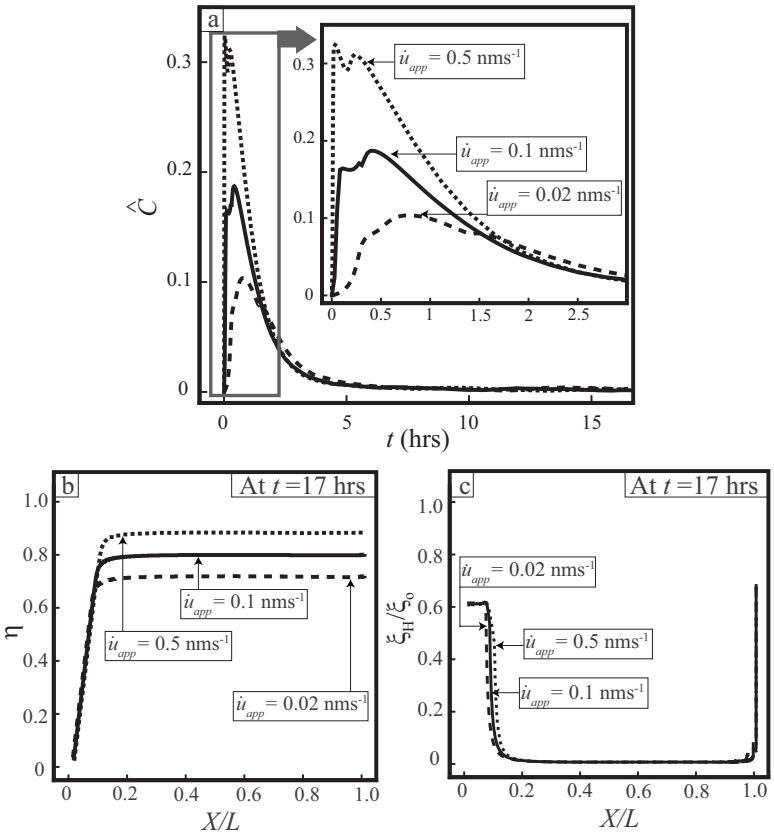

Fig. 9 (*a*) The temporal evolution of $\hat{C}$ in a cell (reference properties) subjected u_{max}=100 nm at three selected values of the applied displacement rate $\dot{u}_{app}$. The corresponding steady-state (t=17 h) distributions of (*b*) stress fiber concentration η and (*c*) focal adhesions as parametrized by ξ_H/ξ_o. The spatial distributions are plotted in terms of the undeformed cell coordinate X.

contractility. The signaling model is based on a biochemical pathway where IP_3 molecules are generated when focal adhesions grow. These IP_3 molecules diffuse through the cytosol leading to the opening of ion channels that disgorge Ca^{2+} from the endoplasmic reticulum leading to the activation of the actin/myosin contractile machinery. The signal pathway thus conceptualized has been coupled with the mechano-sensitive stress fiber and focal adhesion models of Refs. 18, 19, and 17 in order to give an overall model for predicting the stress fiber and focal adhesion responses of cells subjected to mechanical perturbations. A simple numerical example is analyzed where a one-dimensional cell adhered to a rigid substrate is pulled at one end. These simulations indicate that for a realistic range of IP_3 diffusivities, the diffusion of IP_3 is significantly faster than the other cellular processes modeled here, and thus it suffices to model the stress fiber activation signal as spatially uniform. However, the signal levels are sensitive to the nature of the mechanical perturbations (e.g., the rate of loading), and hence the ad hoc signaling models as utilized in our previous studies [17–19,23–25] require careful calibration to specific loading events.

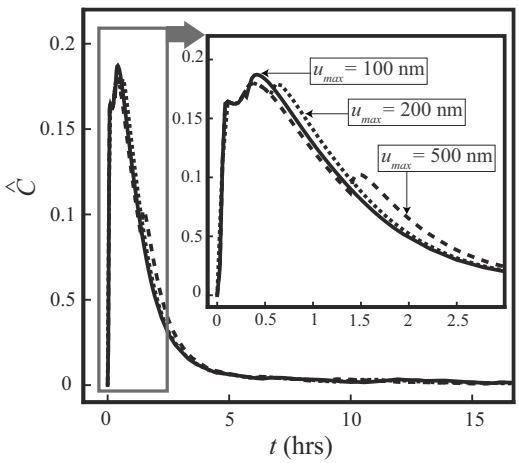

Fig. 10 The temporal evolution of $\hat{C}$ in a cell (reference properties) subjected to a displacement rate $\dot{u}_{app}$=0.1 nm s^{-1} for three selected values of the maximum displacement u_{max}

Previously, the combined stress fiber and focal adhesion models of Refs. [17–19] have been used with a simplified signaling model to simulate successfully a variety of cell responses, including (a) the scaling of the forces exerted by cells on a bed of microneedles [24], (b) the influence of cell shape and boundary conditions on the development of structural anisotropy [19], (c) the high concentration of stress fibers at focal adhesions [19], (d) the formation of stress fibers perpendicular to the direction of cyclic stretch [25], and (e) stress fiber and focal adhesion development on patterned substrates [23]. The signaling model proposed here builds on these results and provides a significant advance toward developing a more comprehensive computational toolbox for simulating the interaction of cells with their mechanical environment.

Acknowledgment

V.S.D. acknowledges the support from the Isaac Newton Trust, Trinity College, Cambridge, UK. A.P. was supported by a Multi University Research Initiative sponsored by the Army Research Office, and R.M.M. and A.G.E. acknowledge this funding that enabled the reported work. R.M.M. was also supported by INM–Leibniz Institute for New Materials.

Appendix A: A Review of Key Biochemical Processes

Here, we describe the key biochemical processes governing (i) cytoskeleton dynamics that generate contractile forces, (ii) focal adhesion dynamics, and (iii) signaling pathways. The focus will be on the relation of the biochemical processes to the mechanical behavior. An overview of the key biochemical processes involved is sketched in Fig. 3, and some of the details given here may be found in general cell biology references such as Ref. [31].

1 Cytoskeletal and Focal Adhesion Dynamics

In the *suspended or resting state*, the binding proteins or integrins are dispersed over the cell surface (and may be attached to some actin filaments). The short actin filaments in the cytoplasm are surrounded by a pool of actin monomers bound to profilin. Myosin II exists in the bent state in which the tail domain interacts with the motor head. *The formation of stress fibers* in the cell is triggered by an activation signal in the form of either a nervous impulse or an external signal that triggers an intracellular signaling cascade. Several parallel intracellular pathways are involved. For example, adhesion to the extracellular matrix triggers a signaling pathway that induces the activity of profilin, cofilin, and gelsolin. In turn, this activates phospholipase C (PLC), which hydrolyzes PIP_2 (phosphatidylinositol 4,5-bisphosphate) and stimulates the release of Ca^{2+} from the endoplasmic reticulum. The influx of Ca^{2+} activates gelsolin, which cleaves the capped actin filaments into tiny fragments. The large numbers of free ends generated in this manner are rapidly elongated by the monomeric actin pool, forming many long filaments, some cross-linked with filamin and some bundled by α-actinin. Phosphorylation triggered by Ca^{2+} causes myosin II to preferentially assume its extended state. This promotes the assembly of myosin II into bipolar filaments that enter into the α-actinin bound actin filament bundles, resulting in the formation of stress fibers. These fibers generate tension by cross-bridge cycling between the actin and myosin filaments. When the tension is allowed to relax, the actin filaments are no longer held in place by the bipolar myosin filaments and the stress fibers disassemble. The biochemomechanical model of Refs. [18,19] captures the essence of the processes described above within a mathematical framework.

The integrin proteins enable a bidirectional control of cell adhesion by dynamically coupling the immobilized matrix and its associated ligands outside the cell with its internal "skeleton" including the stress fibers. Recent studies [32] have elucidated that integrins exist in two conformational states: (i) a low affinity (or bent) state and (ii) an active or a "straight" state with a high affinity to the appropriate ligand. The high affinity integrins interact with the ligand molecules on the ECM and form complexes or bonds, while the "bent" geometry of the low affinity integrins implies that they do not interact with ligand molecules on the ECM [33]. Numerous recent observations suggest that the clustering of the integrins to form focal adhesions is driven by the contractile apparatus *within the cell*, and *not from interactions with the ECM on the outside* [34]. These observations include that the clustering of integrins is weak or nonexistent if (i) the protein that signals the formation of the contractile stress fibers (Rho) is inactive [35], or (ii) 2,3-butanedione monoxime (BDM) is added to the cell to restrict the actin-myosin activity [36]. The model in Ref. [17] proposes a biochemical-mechanical basis for this mechano-sensitivity of the binders coupled to the actin/myosin stress fiber model developed in Refs. [18,19].

2 Biochemical Aspects of Common Signaling Pathways in Cells

Here, we discuss the critical mechanically activated signaling pathways in *nonexcitable* cells such as endothelial cells, blood cells, and fibroblasts. The aim is not to provide a critical review of all the pathways, but rather to give the overall picture of the critical elements that are involved in order to inform the development of a relatively simple modeling approach.

2.1 Focal Adhesions Activate Intracellular Signaling Pathways. Focal adhesions are formed when low affinity mobile integrins in the plasma membrane convert to high affinity integrins and bind with extracellular ligands. When high affinity integrins cluster at focal contacts, the cytoplasmic tyrosine kinase, focal adhesion kinase (FAK), is recruited to focal adhesions by intracellular anchor proteins such as talin, which binds to the integrin β-subunit, or paxillin, which binds to the integrin α-subunit. The clustered FAK molecules cross-phosphorylate each other, creating phosphotyrosine docking sites where Src kinase can bind. Src and FAK now phosphorylate each other and other proteins that assemble in the junction, including many signaling proteins used by receptor tyrosine kinases.

2.2 Receptor Tyrosine Kinases. The phosphorylated tyrosines form docking sites for the PLCγ SH2 domains, bringing PLCγ into proximity with phosphatidylinositol 4,5-biphosphate (PIP_2). The activated γ cleaves PIP_2 to generate two products: inositol 1,4,5-triphosphate (IP_3) and diacylglycerol (DAG). At this step, the signaling pathway splits into two branches: (i) the IP_3 that triggers a release of Ca^{2+} from the ER and (ii) DAG that activates protein kinase C (PKC). We shall focus on the first pathway. Note that the binding of an extracellular signaling molecule to its G-protein linked receptor activates PLCβ. In general, tyrosine kinase activated PLCγ increases Ca^{2+} more slowly and for longer durations that do G-mediated PLCβs [31,37,38].

2.3 IP_3 Diffusion Causes Release of Ca^{2+} Ions From Endoplasmic Reticulum. Inositol 1,4,5-triphosphate (IP_3) is a small water soluble molecule that leaves the plasma membrane and diffuses rapidly through the cytosol. The IP_3 releases Ca^{2+} from the ER by binding to and opening IP_3-gated Ca^{2+}-release channels in the ER membrane. The large electrochemical gradient for Ca^{2+} across this membrane causes Ca^{2+} to escape into the cytosol. The Ca^{2+} concentration in the cytosol is one of the key signals for the initiation of cytoskeletal reorganization, including the formation of stress fibers. The number, affinity, and specificity of Ca^{2+}-binding proteins means that Ca^{2+} is a very localized messenger and diffuses much more slowly than implied by its ionic or hydrated radii; i.e., Ca^{2+} action is local in the cell [37]. Thus, the Ca^{2+} ions are typically associated with the diffusion of IP_3 and can be considered to be supplied at rates determined by the presence of IP_3.

2.4 Restoring Mechanisms. Two key mechanisms operate to bring the Ca^{2+} concentration in the cytosol back to its resting state: (i) IP_3 is de-phosphorylated by specific phosphatases to form IP_2 and IP_4, which closes the Ca^{2+} gates on the ER membrane; (ii) the concentration of Ca^{2+} is brought back to its resting state by Ca^{2+} pumps on the ER membrane that use the energy of ATP hydrolysis to transfer Ca^{2+} from the cytosol into the ER.

2.5 Summary of the Biochemical Signaling Processes Initiated by Mechanical Forces. The application of a mechanical force to the plasma membrane results in the activation of integrins from their low to high affinity states [17]. The biasing of the integrins to their high affinity state generates the signaling cascade described above, generating a Ca^{2+} wave as follows.

(a) IP_3 is produced at the plasma membrane at the location of force application. This IP_3 diffuses through the cytosol.

(b) The rate of calcium release from the ER is proportional to the concentration of IP_3. The resulting locally high concentration of Ca^{2+} in the cytosol reduces further release at those locations, and the pumping of Ca^{2+} back into the ER starts to reduce the local Ca^{2+} concentration.
(c) The high Ca^{2+} concentration initiates the formation of contractile stress fibers that in turn are capable of generating forces on focal adhesions.
(d) This process is repeated at different locations within the cell as the IP_3 wave propagates.
(e) The production of IP_3 at the plasma membrane is terminated when the clustering of integrins is halted.
(f) Closing of the IP_3-gated channels due to the dephosphorylation of IP_3 and the pumping of Ca^{2+} back into the ER refills their stores and reduces the cytoplasmic Ca^{2+} levels back to the resting state.

Appendix B: The One-Dimensional Cytoskeletal Model Accounting for Stress Fiber Contractility

A biochemomechanical model has been devised in Refs. [18,19], which captures the formation and dissociation of stress fibers, as well as the associated generation of tension and contractility. The formation of stress fibers is parametrized by an activation level, designated as $\eta(0 \leq \eta \leq 1)$, defined as the ratio of the concentration of the polymerized actin, and phosphorylated myosin within a stress fiber bundle to the maximum concentrations permitted by biochemistry. The evolution of the stress fibers is characterized by a first order kinetic equation,

$$\dot{\eta} = [1 - \eta]Ck_f - \left(1 - \frac{\sigma}{\sigma_0}\right)\eta k_b \tag{B1}$$

where the overdot denotes time differentiation, while k_f and k_b are the forward and backward rate constants, respectively. In this formula, σ is the tension in the stress fiber bundle, while $\sigma_o \equiv \eta\sigma_{\max}$ is the corresponding isometric stress at the activation level η, with $\sigma_{\max}$ being the tensile stress at full activation ($\eta=1$). The stress fiber formation is initiated by a signaling cascade within the cell. This signal $C(0 \leq C \leq 1)$ (defined as the nondimensional concentration of Ca^{2+}) is the stress fiber activation signal defined in the main body of the paper. The stress σ is related to the fiber contraction/extension strain rate $\dot{\varepsilon}$ by the cross-bridge cycling between the actin and myosin filaments. A simplified (but adequate) version of the Hill-like [39] equation is employed to model these dynamics and is specified as

$$\frac{\sigma}{\sigma_0} = \begin{cases} 0 & \dfrac{\dot{\varepsilon}}{\dot{\varepsilon}_0} < -\dfrac{\eta}{\bar{k}_v} \\ 1 + \dfrac{\bar{k}_v}{\eta}\left(\dfrac{\dot{\varepsilon}}{\dot{\varepsilon}_0}\right) & -\dfrac{\eta}{\bar{k}_v} \leq \dfrac{\dot{\varepsilon}}{\dot{\varepsilon}_0} \leq 0 \\ 1 & \dfrac{\dot{\varepsilon}}{\dot{\varepsilon}_0} > 0 \end{cases} \tag{B2}$$

where the rate sensitivity coefficient, $\bar{k}_v$, is the fractional reduction in fiber stress upon increasing the shortening rate by $\dot{\varepsilon}_0$. Thus, the model treats stress fiber assembly and contractility in a coupled manner via Eqs. (B1) and (B2), respectively.

The constitutive description for the cell is completed by including contributions from passive elasticity, attributed to intermediate filaments and microtubules of the cytoskeleton attached to the nuclear and plasma membranes. These act in parallel with the active elements, whereupon additive decomposition gives the total stress as

$$\Sigma = \sigma + E\varepsilon \tag{B3}$$

for an assumed linear passive response, with E being the Young's modulus and $\varepsilon \equiv \int_0^t \dot{\varepsilon} dt$.

References

[1] Bao, G., and Suresh, S., 2003, "Cell and Molecular Mechanics of Biological Materials," Nature Mater., **2**(11), pp. 715–725.
[2] Chen, C. S., Tan, J., and Tien, J., 2004, "Mechanotransduction at Cell-Matrix and Cell-Cell Contacts," Annu. Rev. Biomed. Eng., **6**(1), pp. 275–302.
[3] Huang, H., Kamm, R. D., and Lee, R. T., 2004, "Cell Mechanics and Mechanotransduction: Pathways, Probes, and Physiology," Am. J. Physiol.: Cell Physiol., **287**(1), pp. C1–C11.
[4] Janmey, P. A., and Weitz, D. A., 2004, "Dealing With Mechanics: Mechanisms of Force Transduction in Cells," Trends Biochem. Sci., **29**(7), pp. 364–370.
[5] Haidekker, M. A., L'heureux, N., and Frangos, J. A., 2000, "Fluid Shear Stress Increases Membrane Fluidity in Endothelial Cells: A Study With Dcvj Fluorescence," Am. J. Physiol. Heart Circ. Physiol., **278**(4), pp. H1401–H1406.
[6] White, C. R., Haidekker, M., Bao, X., and Frangos, J. A., 2001, "Temporal Gradients in Shear, But Not Spatial Gradients, Stimulate Endothelial Cell Proliferation," Circulation, **103**(20), pp. 2508–2513.
[7] Hamill, O. P., and Martinac, B., 2001, "Molecular Basis of Mechanotransduction in Living Cells," Physiol. Rev., **81**(2), pp. 685–740.
[8] Odde, D., Ma, L., Briggs, A., Demarco, A., and Kirschner, M., 1999, "Microtubule Bending and Breaking in Living Fibroblast Cells," J. Cell. Sci., **112**(19), pp. 3283–3288.
[9] Maniotis, A. J., Chen, C. S., and Ingber, D. E., 1997, "Demonstration of Mechanical Connections Between Integrins, Cytoskeletal Filaments, and Nucleoplasm That Stabilize Nuclear Structure," Proc. Natl. Acad. Sci. U.S.A., **94**(3), pp. 849–854.
[10] Helmke, B. P., Rosen, A. B., and Davies, P. F., 2003, "Mapping Mechanical Strain of an Endogenous Cytoskeletal Network in Living Endothelial Cells," Biophys. J., **84**(4), pp. 2691–2699.
[11] Sawada, Y., and Sheetz, M. P., 2002, "Force Transduction by Triton Cytoskeletons," J. Cell Biol., **156**(4), pp. 609–615.
[12] Kaazempur Mofrad, M. R., Abdul-Rahim, N. A., Karcher, H., Mack, P. J., Yap, B., and Kamm, R. D., 2005, "Exploring the Molecular Basis for Mechanosensation, Signal Transduction, and Cytoskeletal Remodeling," Acta Biomater., **1**(3), pp. 281–293.
[13] Adams, W., Pong, T., Geisse, N., Sheehy, S., Diop-Frimpong, B., and Parker, K., 2007, "Engineering Design of a Cardiac Myocyte," J. Comput.-Aided Mater. Des., **14**(1), pp. 19–29.
[14] Wang, Y., Botvinick, E. L., Zhao, Y., Berns, M. W., Usami, S., Tsien, R. Y., and Chien, S., 2005, "Visualizing the Mechanical Activation of Src," Nature (London), **434**(7036), pp. 1040–1045.
[15] Balaban, N. Q., Schwarz, U. S., Riveline, D., Goichberg, P., Tzur, G., Sabanay, I., Mahalu, D., Safran, S., Bershadsky, A., Addadi, L., and Geiger, B., 2001, "Force and Focal Adhesion Assembly: A Close Relationship Studied Using Elastic Micropatterned Substrates," Nat. Cell Biol., **3**(5), pp. 466–472.
[16] Riveline, D., Zamir, E., Balaban, N. Q., Schwarz, U. S., Ishizaki, T., Narumiya, S., Kam, Z., Geiger, B., and Bershadsky, A. D., 2001, "Focal Contacts as Mechanosensors: Externally Applied Local Mechanical Force Induces Growth of Focal Contacts by an Mdia1-Dependent and Rock-Independent Mechanism," J. Cell Biol., **153**(6), pp. 1175–1186.
[17] Deshpande, V. S., Mrksich, M., Mcmeeking, R. M., and Evans, A. G., 2008, "A Bio-Mechanical Model for Coupling Cell Contractility With Focal Adhesion Formation," J. Mech. Phys. Solids, **56**(4), pp. 1484–1510.
[18] Deshpande, V. S., Mcmeeking, R. M., and Evans, A. G., 2006, "A Bio-Chemo-Mechanical Model for Cell Contractility," Proc. Natl. Acad. Sci. U.S.A., **103**(38), pp. 14015–14020.
[19] Deshpande, V. S., Mcmeeking, R. M., and Evans, A. G., 2007, "A Model for the Contractility of the Cytoskeleton Including the Effects of Stress-Fibre Formation and Dissociation," Proc. R. Soc. London, Ser. A, **463**(2079), pp. 787–815.
[20] Icard-Arcizet, D., Cardoso, O., Richert, A., and Hénon, S., 2008, "Cell Stiffening in Response to External Stress Is Correlated to Actin Recruitment," Biophys. J., **94**(7), pp. 2906–2913.
[21] Veigel, C., Molloy, J. E., Schmitz, S., and Kendrick-Jones, J., 2003, "Load-Dependent Kinetics of Force Production by Smooth Muscle Myosin Measured With Optical Tweezers," Nat. Cell Biol., **5**(11), pp. 980–986.
[22] Besser, A., and Schwarz, U. S., 2007, "Coupling Biochemistry and Mechanics in Cell Adhesion: A Model for Inhomogeneous Stress Fiber Contraction," New J. Phys., **9**, p. 425.
[23] Pathak, A., Deshpande, V. S., Mcmeeking, R. M., and Evans, A. G., 2008, "The Simulation of Stress Fibre and Focal Adhesion Development in Cells on Patterned Substrates," J. R. Soc., Interface, **5**(22), pp. 507–524.
[24] Mcgarry, J. P., Fu, J., Yang, M. T., Chen, C. S., Mcmeeking, R. M., Evans, A. G., and Deshpande, V. S., 2009, "Simulation of the Contractile Response of Cells on an Array of Micro-Posts," Philos. Trans. R. Soc. London, Ser. A, **367**(1902), pp. 3477–3497.
[25] Wei, Z., Deshpande, V. S., Mcmeeking, R. M., and Evans, A. G., 2008, "Analysis and Interpretation of Stress Fiber Organization in Cells Subject to Cyclic Stretch," ASME J. Biomech. Eng., **130**(3), p. 031009.
[26] Allbritton, N., Meyer, T., and Stryer, L., 1992, "Range of Messenger Action of Calcium Ion and Inositol 1,4,5-Trisphosphate," Science, **258**(5089), pp. 1812–

1815.
[27] Jafri, M. S., and Keizer, J., 1995, "On the Roles of Ca^{2+} Diffusion, Ca^{2+} Buffers, and the Endoplasmic Reticulum in Ip3-Induced Ca^{2+} Waves," Biophys. J., **69**(5), pp. 2139–2153.
[28] Wagner, J., and Keizer, J., 1994, "Effects of Rapid Buffers on Ca^{2+} Diffusion and Ca^{2+} Oscillations," Biophys. J., **67**(1), pp. 447–456.
[29] Galbraith, C. G., Yamada, K. M., and Sheetz, M. P., 2002, "The Relationship Between Force and Focal Complex Development," J. Cell Biol., **159**(4), pp. 695–705.
[30] Jungbauer, S., Gao, H., Spatz, J. P., and Kemkemer, R., 2008, "Two Characteristic Regimes in Frequency-Dependent Dynamic Reorientation of Fibroblasts on Cyclically Stretched Substrates," Biophys. J., **95**(7), pp. 3470–3478.
[31] Alberts, B., Johnson, A., Lewis, J., Raff, M., Roberts, K., and Watson, J. D., 2002, *Molecular Biology of the Cell*, Garland, New York.
[32] Carman, C. V., and Springer, T. A., 2003, "Integrin Avidity Regulation: Are Changes in Affinity and Conformation Underemphasized?," Curr. Opin. Cell Biol., **15**(5), pp. 547–556.
[33] McCleverty, C. J., and Liddington, R. C., 2003, "Engineered Allosteric Mutants of the Integrin $\alpha M\beta 2$ I Domain: Structural and Functional Studies," Biochem. J., **372**(1), pp. 121–127.
[34] Burridge, K., and Chrzanowska-Wodnicka, M., 1996, "Focal Adhesions, Contractility and Signaling," Annu. Rev. Cell Dev. Biol., **12**(1), pp. 463–519.
[35] Hotchin, N., and Hall, A., 1995, "The Assembly of Integrin Adhesion Complexes Requires Both Extracellular Matrix and Intracellular Rho/Rac Gtpases," J. Cell Biol., **131**(6), pp. 1857–1865.
[36] Tan, J. L., Tien, J., Pirone, D. M., Gray, D. S., Bhadriraju, K., and Chen, C. S., 2003, "Cells Lying on a Bed of Microneedles: An Approach to Isolate Mechanical Force," Proc. Natl. Acad. Sci. U.S.A., **100**(4), pp. 1484–1489.
[37] Clapham, D. E., 1995, "Calcium Signaling," Cell, **80**(2), pp. 259–268.
[38] Clapham, D. E., 2007, "Calcium Signaling," Cell, **131**(6), pp. 1047–1058.
[39] Hill, A. V., 1938, "The Heat of Shortening and the Dynamic Constants of Muscle," Proc. R. Soc. London, Ser. B, **126**(843), pp. 136–195.